



Semi Empirical Model of Global Warming Including Cosmic Forces, Greenhouse Gases, and Volcanic Eruptions

Antero Ollila^{1*}

¹*Department of Civil and Environmental Engineering (Emer.), School of Engineering, Aalto University, Espoo, Finland.*

Author's contribution

The sole author designed, analyzed, interpreted and prepared the manuscript.

Article Information

DOI: 10.9734/PSIJ/2017/34187

Editor(s):

(1) Mohd Rafatullah, Division of Environmental Technology, School of Industrial Technology, Universiti Sains Malaysia, Malaysia.

(2) Abbas Mohammed, Blekinge Institute of Technology, Sweden.

Reviewers:

(1) José Martínez Reyes, Trajectory of Engineering in Energy, University of the Ciénega of Michoacán State, México.

(2) Francisco Bulnes, Department In Mathematics And Engineering, Technological Institute of High Studies of Chalco, Mexico.

(3) Shu-Lung Kuo, Department of Environ, Engineering & Science, Open University of Kaohsiung, Taiwan.

(4) A. Ayeshamariam, Department of Physics, Khadir Mohideen College, India.

(5) Jorge F. Carrasco, University of Magallanes, Chile.

Complete Peer review History: <http://www.sciencedomain.org/review-history/19828>

Original Research Article

Received 17th May 2017

Accepted 28th June 2017

Published 3rd July 2017

ABSTRACT

In this paper, the author describes a semi empirical climate model (SECM) including the major forces which have impacts on the global warming namely Greenhouse Gases (GHG), the Total Solar Irradiance (TSI), the Astronomical Harmonic Resonances (AHR), and the Volcanic Eruptions (VE). The effects of GHGs have been calculated based on the spectral analysis methods. The GHG effects cannot alone explain the temperature changes starting from the Little Ice Age (LIA). The known TSI variations have a major role in explaining the warming before 1880. There are two warming periods since 1930 and the cycling AHR effects can explain these periods of 60 year intervals. The warming mechanisms of TSI and AHR include the cloudiness changes and these quantitative effects are based on empirical temperature changes. The AHR effects depend on the TSI, because their impact mechanisms are proposed to happen through cloudiness changes and TSI amplification mechanism happen in the same way. Two major volcanic eruptions, which can be detected in the global temperature data, are included. The author has reconstructed the global temperature data from 1630 to 2015 utilizing the published temperature estimates for the period

*Corresponding author: E-mail: aveollila@yahoo.com;

1600 – 1880, and for the period 1880 – 2015 he has used the two measurement based data sets of the 1970s together with two present data sets. The SECM explains the temperature changes from 1630 to 2015 with the standard error of 0.09°C, and the coefficient of determination r^2 being 0.90. The temperature increase according to SCEM from 1880 to 2015 is 0.76°C distributed between the Sun 0.35°C, the GHGs 0.28°C (CO₂ 0.22°C), and the AHR 0.13°C. The AHR effects can explain the temperature pause of the 2000s. The scenarios of four different TSI trends from 2015 to 2100 show that the temperature decreases even if the TSI would remain at the present level.

Keywords: Climate change; climate model; cosmic forces; global warming; greenhouse gases.

1. INTRODUCTION

The Intergovernmental Panel on Climate Change (IPCC) has published five assessment reports (AR) about the climate change. According to IPCC the climate change is almost totally due to the concentration increases of GH gases (97.9%) since the industrialization 1750. The Radiative Forcing (RF) value of the year 2011 corresponds the temperature increase of 1.17°C, which is 37.6% greater than the observed temperature increase 0.85°C [1]. Because of the temperature pause since 2000, the error of this model is now about 49%. This great error of the IPCC's model means that the

approach of IPCC can be questioned. One obvious reason is that IPCC mission is limited to assess only human-induced climate change. In this paper, other climate changing forces Greenhouse Gases (GHG), the Total Solar Irradiance (TSI), the Astronomical Harmonic Resonances (AHR), and the Volcanic Eruptions (VE), are analyzed and their impacts on the global temperature are quantified on the theoretical and empirical ways. The objective of this paper is to construct a global temperature data set from 1610 to 2015 and to combine the above listed climate change forces on the theoretical and empirical grounds to explain the temperature changes during this period.

Table 1. List of symbols, abbreviations, and acronyms

Acronym	Definition
AGW	Anthropogenic global warming
AHR	Astronomic harmonic resonances
AR	Assessment report of IPCC
Barycenter	Gravity center of the solar system
CF	Cloud forcing
CS	Climate sensitivity
CSP	Climate sensitivity parameter ($=\lambda$)
ECS	Equilibrium climate sensitivity
GCR	Galactic cosmic rays
GH	Greenhouse
GHG	GH gas
GISS	Goddard Institute for Space Studies
HadCRUT4	Temperature data set of Hadley Centre
IPCC	The Intergovernmental Panel on Climate Change
ISCCP	International Satellite Cloud Climatology Project
LIA	Little ice age
NH	Northern hemisphere
RF	Radiative forcing change
SECM	Semi empirical climate model
SH	Southern hemisphere
TCS	Transient climate sensitivity
T-est	Proxy temperature estimate
T-rec	Measured temperature
T-comp	T-est + T-rec
UAH	University of Alabama in Huntsville
VE	Volcanic eruptions

Table 1 includes all the symbols, abbreviations, acronyms, and definitions used repeatedly in this paper.

2. CONSTRUCTION OF THE GLOBAL TEMPERATURE FROM 1610 TO 2015

2.1 Estimated Global Temperature from 1610 to 1890

There is no generally accepted temperature data for the period from 1610 to 1890 because there have been no global temperature recording methods available. Therefore, all the global temperatures for this period are estimated using different proxy methods. The author has selected three commonly used proxy data sets namely Briffa et al. [2] applying tree ring density data, Moberg et al. [3] applying tree ring data and lake and ocean sediment data, and Ljungqvist [4] applying nine different proxy methods. The data sets are normalized to give zero Celsius degrees for the period from 1877 to 1883, because the year 1880 is generally used as a starting point for the recorded temperatures. The three data sets and the average data set is depicted in Fig. 1.

All three temperature graphs show the same kind of overall trend from 1610 to 1890. The temperature decrease caused by the Tambora

eruption in 1815 can clearly be seen but the Krakatoa temperature decrease is significantly smaller. It appears that the graph of Briffa et al. [2] is the most sensitive for temperature changes. It is natural that the graph of Ljungqvist [4] is the most insensitive in regard to changes because the averaging of the nine different proxies smoothens out the changes. The arithmetical average of these three different proxy temperatures may be a good compromise regarding sensitivity for temperature changes.

The three data sets applied cover the northern hemisphere (NH) only. The NH and SH satellite data sets of the University of Arizona in Huntsville (UAH) [5] shows that the difference of the average values from 1980 to 2015 is only 0.013°C. This small difference means that it is justified to use NH temperatures as the global temperature change as well.

2.2 Recorded Global Temperature from 1880 to 2015

HadCrut4 [6] temperature data set starts from 1850 but the coverage of the data is not very good. A special problem has been detected in different data set versions of GISS [7]. The versions of the year 2000 and 2016 of this data and the satellite temperature data set of UAH are depicted in Fig. 2.

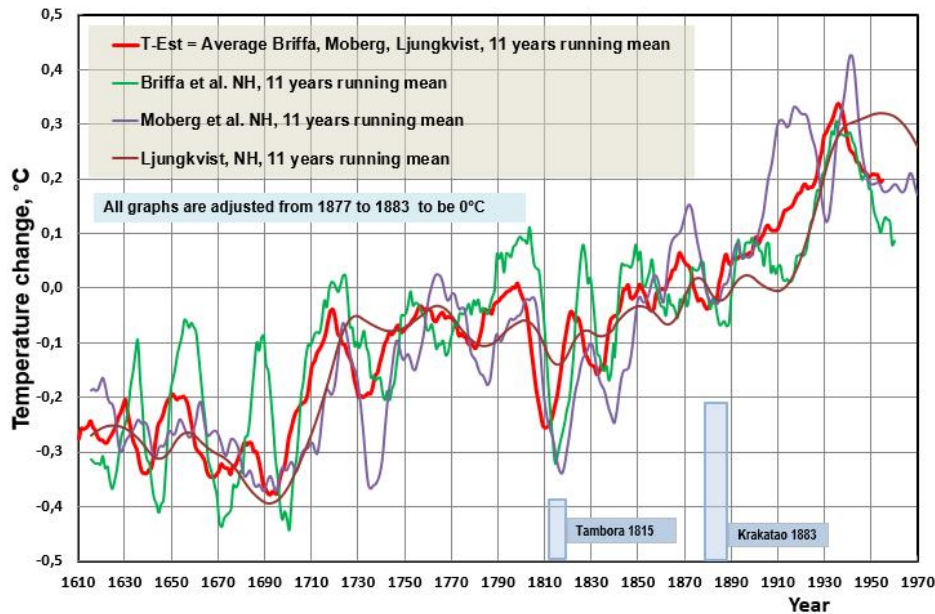


Fig. 1. Estimated global temperature T-Est constructed as the average of three temperature proxies

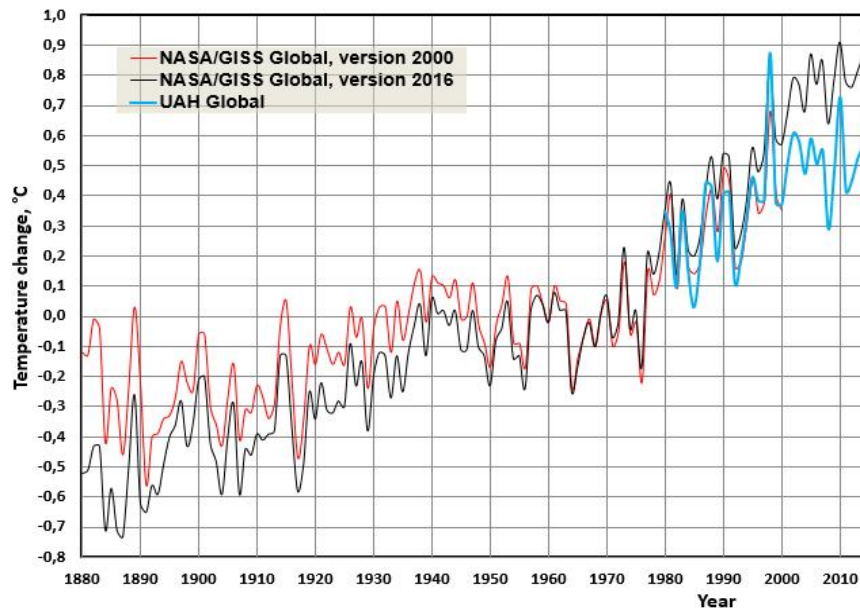


Fig. 2. The temperature data versions 2000 and 2016 of NASA/GISS [7] and UAH [5]

The temperature increase from 1880 to 2000 has been 0.47°C according to GISS version 2000, and the increase for the same period has been 1.09°C according to version 2016. As one can see in Fig. 2, the version 2016 (GISS-16) temperature in 1880 has been much lower but the temperature in 2000 is higher than the one of the version 2000. Also, the average temperature of GISS-16 [7] during the period from 2000 to 2015 is 0.26°C higher than that of UAH [5]. These new versions have been adjusted in the name of data homogenization. Another suspicious element in the GISS data sets is the warming during 1930s. The extreme weather events like heat waves and draughts in USA [8,9] related to high temperatures show that in 1930s these events have been stronger and more frequent than during the 2000s. Therefore, the author has been looking for older data before 1979, which was the starting year of UAH temperature data set.

In 1974, the Governing Board of the National Research Council of USA established a Committee for the Global Atmospheric Research Program. This committee consisted of tens of the front-line climate scientists in USA and their major concern was to understand in which way the changes in climate could affect human activities and even life itself. A stimulus for this special activity was not the increasing global temperature but the rapid temperature decrease since 1940. There was a common threat of a

new ice age. The committee published in behalf of National Academy of Sciences the report [10] by name "Understanding Climate Change – A Program for Action" in 1975. The committee had used the temperature data published by Budyko [11], which shows the temperature peak of 1930s and cooling to 1969. This digitized temperature graph from 1880 to 1969 is depicted in Fig. 3. The temperature peak of 30s is little bit lower in the graph published by Hansen [12]. There is another global data graph published by Angell and Korshover [13] from 1957 to 1975 following the trend of Budyko [11] but because it so short a period, it has not been used. In constructing the recorded global temperature data set T-rec, the author has used the average of Budyko [11] and Hansen [12] data from 1880 to 1969. The temperature change from 1969 to 1979 is covered by the GISS-16 data and thereafter by UAH [5]. The UAH data has been normalized to GISS-16 [7] by equaling the average values from 1979 to 1981. All these data set values are depicted in Fig. 3.

The constructed data set T-rec is normalized by averaging the decade 1880 to be same as that of T-est. The constructed T-rec shows the peak value of 1930s to be about 0.25°C lower than the 2000s. The same difference in the GISS-00 (version 2000) is about 0.3°C and in the GISS-16 version the difference is about 0.6°C . As references, there are GISS-16 [7] and HadCrut4 [6] temperature graphs also depicted in Fig. 3.

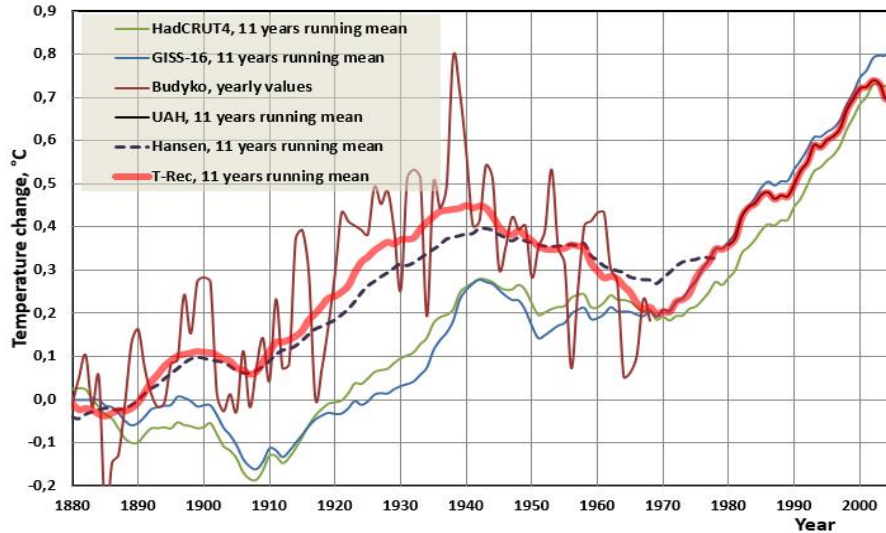


Fig. 3. The different recorded temperature data set and the constructed data set T-rec

The difference between these data sets and T-rec is even 0.35°C during the period from 1880 to 1950. In the late 1970s the differences between different data sets are almost neglectable, when the present warming was in the early phase. A general conclusion is that the history (1880-1960) of the global temperature of the new versions of GISS is getting colder and the newer temperatures of 2000s are getting warmer. These changes, which happen always in the newer versions of GISS, arouse doubts of justification of these changes. Soon et al. [14] have analyzed that the rural land-based meteorological stations data results into a temperature trend, which deviate from the official temperature trends especially during 30s, it is very close to T-rec calculated in this study. Their conclusion is that the urban heat island syndrome of meteorological stations has caused a bias into the measurement data. Therefore, the author considers that the T-rec constructed from the older global temperature data sets is more reliable than the GISS [5] and HadCRUT4 [7] temperature data. The combination of the T-est and T-rec is labelled as T-comp, which is valid from 1630-2015.

3. DEVELOPMENT OF SEMI EMPIRICAL CLIMATE MODEL (SECM)

3.1 Temperature Impacts of Greenhouse Gases (GHG)

According to IPCC¹ the climate change is almost totally due to the concentration increases of GH

gases since the industrialization 1750 and the global warming can be calculated using Eq. (1) [15]:

$$dT = \text{CSP} * \text{RF} \quad (1)$$

Where dT is the temperature change (K) since 1750, CSP (also marked by λ) is a climate sensitivity parameter (K/Wm^{-2}) and RF is radiative forcing (Wm^{-2}) caused by GH gases and other drivers. The total RF in AR5 [15] was 2.34 Wm^{-2} in 2011 and the RF value of solar irradiance was 0.05 Wm^{-2} , which means 2.1% positive contribution. The CSP is nearly invariant parameter according to IPCC [15] having a typical value about $0.5 \text{ K}/(\text{Wm}^{-2})$.

The transient climate sensitivity (TRC) according to Eq. (1) and the RF value of 3.7 Wm^{-2} for CO_2 is 1.85°C [16] and it is close to the average TRC 1.75°C (from 1.0°C to 2.5°C) reported in the AR5 [1]. The equilibrium climate sensitivity (ECS) reported in AR5 [1] is in the range 1.5°C to 4.5°C , which means the average ECS to be 3.0°C . Several researchers have reported much lower ECS values than 3.0°C (the best estimates / the minimum values): Aldrin [17] $2.0^{\circ}\text{C} / 1.1^{\circ}\text{C}$; Bengtson & Schwartz [18] $2.0^{\circ}\text{C} / 1.15^{\circ}\text{C}$; Otto et al. [19] $2.0^{\circ}\text{C} / 1.2$, and Lewis [20] $1.6^{\circ}\text{C} / 1.2^{\circ}\text{C}$. In the above referred studies the RF [16] value of 3.7 Wm^{-2} for CO_2 has been used. It means that the CSP values of these studies are essentially lower than $0.5 \text{ K}/\text{Wm}^{-2}$ and it means that there is no positive water feedback. Harde [21] has used spectral analysis methods and the

two-layer climate model in calculating the ECS values and his result is 0.6°C. Ollila [22] has also reported the ECS value of 0.6°C by utilizing spectral analysis and no water feedback in CSP and in RF formula:

$$dT = 0.27 \text{ K}/(\text{Wm}^{-2}) * 3.12 * \ln(\text{CO}_2/280) \quad (2)$$

Where CO₂ is the actual CO₂ concentration (ppm). The warming effect of CO₂ according to Eq. (2) until to 2015 is 0.28°C. Ollila [23] has shown that the total precipitable water (TPW) changes are neglectable from 1979 to 2015 challenging the assumption of the constant relative humidity assumption of IPCC. Ollila [24] has combined the warming effects of CH₄ and N₂O into one linear equation based on the spectral analysis calculations:

$$dT = -0.5558 + 0.0003176 * \text{Year} \quad (3)$$

The temperature increase by CH₄ and N₂O from 1750 to 2015 is 0.083°C according to Eq. (3).

3.2 Temperature Impacts of Total Solar Irradiance (TSI) Changes

The second element in the SECM is TSI (Total Solar Irradiance) changes caused by activity variations of the Sun. The TSI changes have been estimated by applying different proxy methods. Lean [25] has used sunspot darkening and facular brightening data. Hoyt and Schatten [26] have used three different indices namely sunspot structure, solar cycle, and equatorial

solar rotation rate data. Bard [27] has used isotopes ¹⁴C and ¹⁰Be production rates in evaluating the solar magnetic variability. These TSI trends based on these three methods are depicted in Fig. 4. There are similarities and differences between these three trends.

The author has selected the data set of Lean [25], which is available to 2000 and combined this data to the data of PMOD data set [28] from 2000 onward. According to this data, TSI has increased 2.75 Wm² since the 1650's as depicted in Fig. 4. The direct warming impact can be calculated by Eq. (4) derived from the Earth's energy balance

$$T = (\text{TSI} * (1 - \alpha) / 4s)^{0.25} \quad (4)$$

where α is the Earth's total albedo, and s is Stefan-Boltzmann constant. The dependency of the Earth's albedo on the cloudiness can be calculated based on the three pairs of cloudiness and albedo values [29]. Cloudiness-% values are 0%, 66%, and 100%. The cloudiness-% of 66 is the average all-sky value of the present climate. The corresponding albedo values can be calculated according to the albedo specification by dividing the total reflected shortwave radiation flux by the total solar radiation flux (324 Wm⁻²): 53/342, 104.2/342, and 120/342). These three pairs of data are fitted to the second order polynomial:

$$\alpha = 0.15497 + 0.0028623 * \text{cloudiness-\%} - 0.000009 * (\text{cloudiness-\%})^2 \quad (5)$$

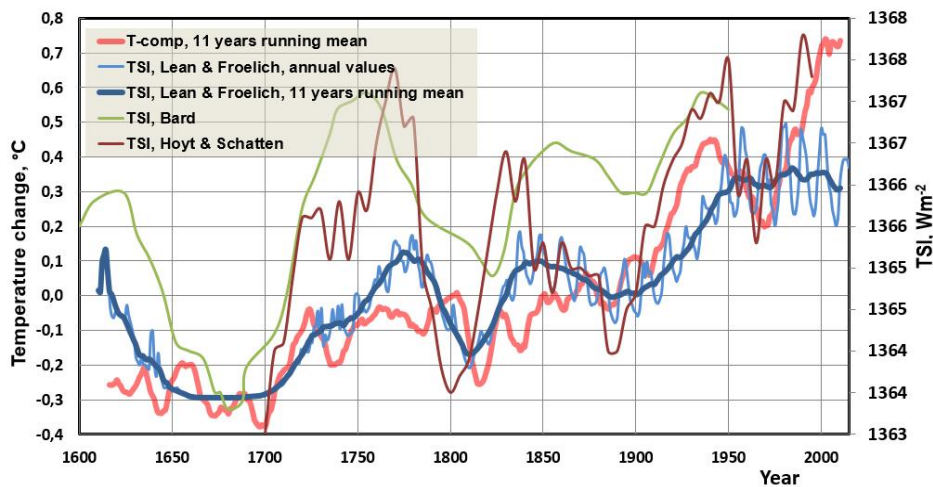


Fig. 4. TSI from 1610 to 2014 Lean [25], PMOD [28], Bard [27] and Hoyt and Schotten [26] and the global temperature T-Comp

McIntyre & McKittrick [30], Alley [31], Ljungvist [4], and Esper et al. [32] have come into conclusion that there have been at least two warm periods about 1000 and 2000 years ago. The direct irradiance changes have not been big enough to explain these changes, because the direct temperature impact by TSI change from 1650 to 2015 is 0.12°C. In the pioneer research Svensmark [33] has introduced evidence about the phenomena in which solar cycle variations modulate galactic cosmic ray (GCR) fluxes in the earth's atmosphere, which phenomenon could cause clouds to form. They argued that cosmic ray particles collide with particles in atmosphere, inducing electrical charges on them and nucleating clouds. Svensmark et al. [34] have found further evidences about this mechanism by studying the coronal mass ejections from the Sun. They found that low clouds contain less liquid water following cosmic ray decreases caused by the Sun. This mechanism amplifies the impacts of the original changes in the Sun's activity on the Earth's climate but the researchers have not been able to calculate the quantitative effects of TSI changes.

The author has calculated the empirical warming effects of TSI changes on the three periods: 1665 – 1703, 1844 – 1873, and 1987-1991, see Table 2. The periods are selected so that the positive and negative temperature effects of Astronomic Harmonic Resonances (AHR) during these periods compensate each other, see section 4. The first period acts as a reference period, when the warming impacts of the Sun are zero. The observed temperature changes caused by the TSI changes during the two other periods are calculated by subtracting the dT caused by the GH gases from the observed dT-comp. The cloudiness-% of the selected periods are calculated applying Eq. (4) and Eq. (5). The cloudiness-% of 1987-1991 is practically same as the one from the ISCCP data set [35].

Table 2. TSI, albedo, cloudiness, and temperature changes during three periods

Period	TSI, Wm ⁻²	dT, °C	Albedo	Cloud.- %
1665-1703	1363.45	0.0	0.308807	68.5
1844-1873	1365	0.24	0.306988	67.4
1987-1991	1366.2	0.50	0.304343	66.0

The relationship between the temperature change and the cloudiness-% change can be fitted by the 2. order polynomial, which is slightly nonlinear:

$$\text{cloudiness-\%} = -457777.75 + 671.93304 * \text{TSI} - 0,2465316 * \text{TSI}^2 \quad (6)$$

Where cloudiness-% change depends on the TSI change. During the analyzed period from 1630-2015 the corresponding albedo and temperature changes are calculated by Eq. (4) and Eq. (5). The temperature change of 0.50°C caused by TSI change of 2.67 Wm⁻² can be divided between the direct impact of TSI change 0.12°C and the cloudiness-% decrease of 2.67% causing the temperature increase of 0.38°C. Cloud forcing according to Eq. (4) and Eq. (5) is 1.7°C/cloudiness-% and this relationship is included in Eq. (6). In this analysis, the cloudiness-% decrease from 68.5 to 66 explains the amplification of TSI increase. Because we do not have real cloudiness measurements before 1980, we do not know exactly what have been the real cloudiness variations before that year. Kauppinen et al. [36] and Ollila [29] have reported that the cloudiness forcing is -0.1 °C/cloudiness-% using two different approaches. According to this cloud forcing, the cloudiness-% change needed to explain the temperature change would be from 69.45 to 66.0. Anyway, the empirical result is that the relatively small cloudiness changes can explain, why the temperature effect of the TSI changes are amplified by a factor = 0.5°C / 0.12°C = 4.2.

3.3 Temperature Impacts of Astronomical Harmonic Resonances (AHR)

The third element of the SECM is a phenomenon called Astronomical Harmonic Resonances (AHR). This approach has proposed Scafetta [37]. He found that large climate oscillations with peak-to-trough amplitude of about 0.1°C and 0.25°C, and periods of about 20 and 60 years, respectively, are synchronized to the orbital periods of Jupiter (29.4 years) and Saturn (11.87) years.

Ermakov et al. [38] have proposed that the influence mechanism of the AHR happens through the variations of space dust entering the Earth's atmosphere. The estimates of daily dust amount vary from 400 to 10000 tons. The optical measurement of the Infrared Astronomical Satellite (IRAS) revealed in 1983 that the Earth is embedded in a circumsolar toroid ring of dust

[39], Fig. 5. This dust ring co-rotates around the Sun with Earth and it locates from 0.8 AU to 1.3 AU from the Sun [40].

In the wake of the Earth is the permanent trail of dust particles having about 10% greater density than the background zodiacal cloud. The darker spots in Fig. 5 represent higher concentrations of dust. Gold [39] has pointed out that the small particles in the Solar System spiral toward the Sun but they may become trapped in resonances with the planets. This should result the circumsolar dust cloud, which is not uniform. Dermott et al. [41] have shown by numerical simulations that the trailing density of the cloud is higher than the leading density and this is confirmed by the IRAS quantitative measurements. Simulations show that the dust particles are trapped in a 5:6 resonance with the Earth with the results that their paths are not symmetric about the Sun-Earth line. According to Dermott et al. [41] this asymmetric nature of the heliocentric dust

cloud leads to greater dust amount encountering the Earth during September-October when the Earth is closest to the trailing cloud.

Variations in dust amounts happen during a longer time scale depending on the periodicities of the planets, which can move the dust cloud position in the Earth's orbit. Scafetta [37] has proposed that the climate can also be directly influenced by the magnetic field oscillations caused by the perturbations of the planets. AHR resonance, collective synchronization and feedback mechanisms could amplify the effects of a weak external periodic forcing. In the same way that galactic cosmic rays (GCR) cause ionization in the atmosphere, dust particles can do the same phenomenon. In this respect, the cosmic ray model and the cosmic dust model have a common meeting point but the original reasons are different: The Sun activity changes and planetary periodical motions as illustrated in Fig. 6.

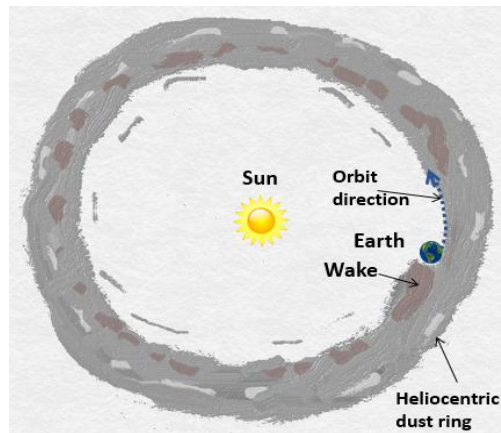


Fig. 5. A schematic picture of the circumsolar dust cloud reproduced by the author according to the presentation of the numerical simulations [40]

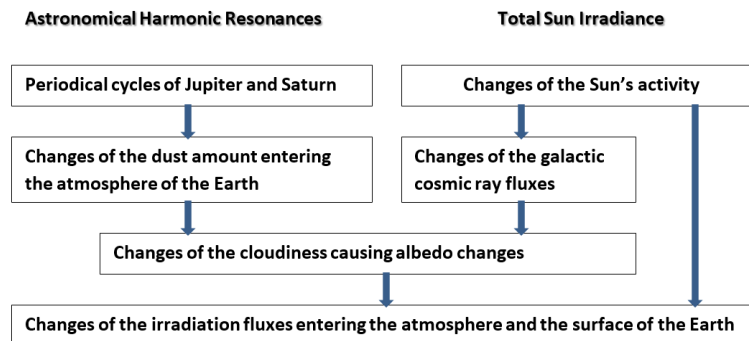


Fig. 6. The influence mechanisms of TSI changes and Astronomic Harmonic Resonances (AHR)

Ollila [24] has analyzed that using the graphical data of Ermakov et al. [38] and the GH gas warming effects, the correlation between the combined model (AHR, TSI and GH gases) and the real temperature data is very good with the coefficient of correlation r^2 being 0.957 from 1880 to 2015. The calculated correlation in this case is not based on the quantified warming effects of AHR and TSI. The major objective of this paper is to assess the quantified effects AHR and TSI changes on the global temperature starting from the LIA. The periodicities caused by Jupiter and Saturn can be found in the calculated speed variations of the Sun around the Solar System Barycenter (SSB). The author has used the Horizon's application of NASA [42] in depicting the graphs in Fig. 7.

In Fig. 7 is also depicted the variations of the maximum speed values (blue line) of the 20 years' cycles. This graphical line is 11 years running average. It should be noticed that the speed variations are not fully symmetric around the average speed and thus the temperature effects are also asymmetric. The 60-year's cycle can be easily detected. These temperature effects of the AHR changes are based on the speed changes of the Sun. The magnitude of the AHR effect is calculated on the empirical basis. The change from 1941 peak temperature $+0.185^\circ\text{C}$ to the minimum temperature -0.15°C in 1962 is used to estimate the AHR impact:

$$dT = -6.43125 + 418.75 * SS \quad (7)$$

Where dT ($^\circ\text{C}$) is the temperature change and SS is the Sun speed (kms^{-1}).

Because the TSI variations and the AHR variations finally happen through the cloudiness changes, these effects cannot be summarized directly. The average cloudiness-% according to ISCCP [35] is about 66% and the average cloud layer is from 1.6 km to 4.0 km [43]. When the low activity of the Sun has increased cloudiness to its maximum value, the cloudiness growth by nucleation process increase cannot increase the cloudiness anymore. It means that 1) the humidity in the atmosphere is not adequate to increase the cloudiness area over the drier areas of the globe even though the nucleation process has increased or 2) the AHR actually changes the thickness and the mass of the existing clouds but these changes do not change the area of the clouds. When the Sun's activity is in maximum, the cloudiness changes by AHR can have a full effect, because in these conditions the nucleation process controls the amount of cloudiness. In

calculating this relationship, the author has used a factor, which has a sinusoidal dependency on the TSI value: TSI of 1363.43 Wm^{-2} during the LIA gives factor value zero and the TSI value of 1366.2 Wm^{-2} during the present maximum gives the value = 1. The sinusoidal dependency smoothens the changes close to the maximum and the minimum TSI fluxes.

3.4 Temperature Impacts of Major Volcanic Eruptions (VE)

The strong volcanic eruptions, which have the Volcanic Explosivity Index (VEI) 5 or 6, have capacity to create eruption columns reaching the stratosphere [44]. The best documented eruption of this kind was the Mt. Pinatubo eruption in 1991. The aerosol cloud covered the latitudes from 60S to 60N after three months and in six months the cloud was uniform over the hemispheres [45]. These kinds of eruptions typically reduce the global temperature by 0.5°C from 2 to 5 years. During the period from 1600 to 2015 there has been four volcanic eruptions with VEI index 5-7 namely Tambora 1815, Krakatoa 1883, Novarupta 1912, and Pinatubo 1991. In the global temperature record constructed in this research, the eruptions of Tambora and Krakatoa can be identified but the Novarupta ja Pinatubo effects disappear in the 11 years running mean presentation. The temperature effects of both eruptions have been estimated in the same way. The temperature decrease starting from the eruption year and the consecutive years have been -0.5°C , -0.35°C , -0.1°C , and -0.05°C .

3.5 The Summary of the SECM Temperature Effects

The estimated and observed temperature T_{comp} and the temperature by the SECM are depicted in Fig. 8. All temperatures are smoothed by 11 years running average. The average values of the SECM and T_{comp} are normalized to be the same for the period from 1630 to 2015. This figure shows that the global temperature does not follow the monotonically increasing temperature effect of GH gases. The major driver of the climate change is the Sun. The AHR explain the strong temperature peaks of 30's and the now in 2000's. Without the AHR effects the total explanation power of SECM would be much weaker since 1900. Because the temperature effects depend on the Sun activity, the magnitude of AHR effects disappears totally in 1600s. The coefficient of correlation $r^2 = 0.90$ for the period from 1630 to 2015 and the standard error of estimate is 0.09°C .

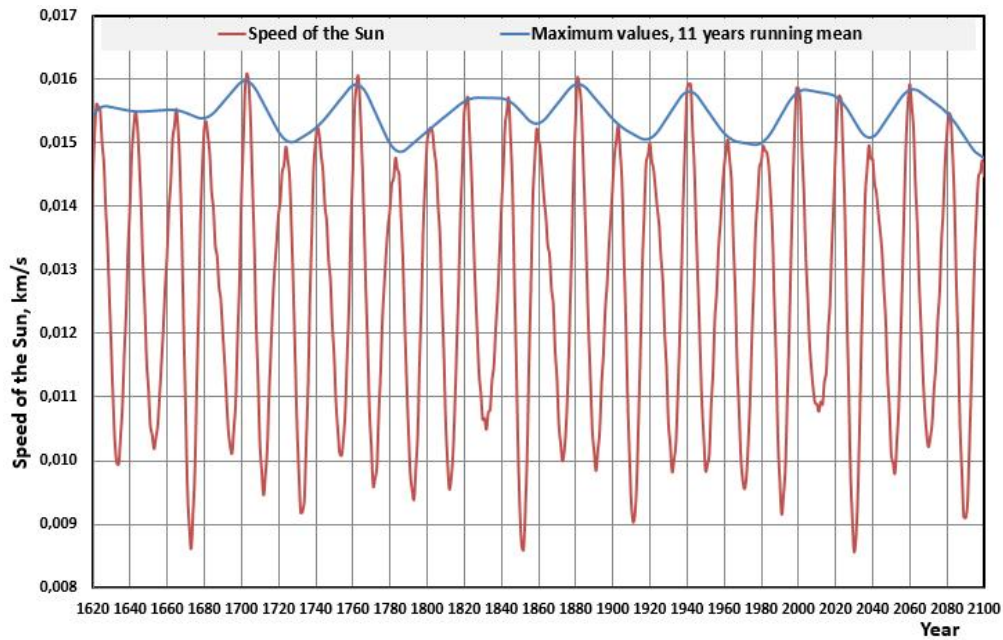


Fig. 7. The speed variations of the sun around the solar system Barycenter

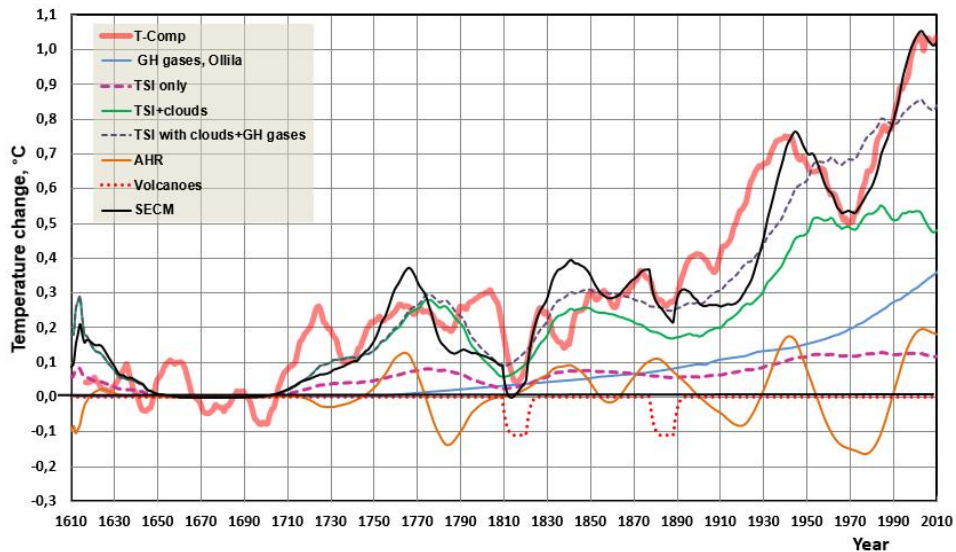


Fig. 8. The estimated and observed temperature T-comp and the temperature by SECM. All temperatures are smoothed by 11 years running mean

The average contributions of the different climate forcing elements during the centuries and in year 2015 have been summarized in Table 3.

The Sun's contribution is the greatest but the warming effect of GHGs is steadily increasing having the impact of 37.3% in 2015. The average contribution of AHRs is zero in the long run but

during the shorter periods they may be positive or negative.

3.6 The Future Temperature Scenarios by the SECM

The possible scenarios depending on the future changes in the Sun's activity can be easily

calculated using the SECM. The author has selected four different scenarios with different decreasing TSI trends in 35 years: Scenario 1, TSI decrease -3 Wm^{-2} ; scenario 2, TSI decrease -2 Wm^{-2} ; scenario 3, TSI decrease -1 Wm^{-2} ; scenario 4, TSI decrease 0 Wm^{-2} . After the decrease phase, the TSI flux stays at the same level to 2100. These scenarios are depicted in Fig. 9.

The behavior of the Sun has been difficult to predict for researchers. The two dynamos model of the Sun developed by Shepherd et al. [46] explains very well the Sun's activity during the last three solar cycles. This model predicts that the Sun's activity approaches the conditions, where the Sun spots disappear almost totally during the next two solar cycles like during the Maunder minimum. The AHR effect explains, why the present temperature pause has continued so long, because the positive peak duration is exceptionally long, Fig. 7. Because the AHR effect also turn to a decreasing phase after 2020, the temperature would start to gradually decrease regardless of the Sun's activity change trend. In Fig. 9 the temperatures according to the IPCC model are depicted for the years 2005, 2011 and 2016. The error in comparison to the observed temperature is very clear and if the temperature does not increase in the coming years, the error is becoming intolerable.

4. DISCUSSION

The constructed average global temperature T_{comp} is a combination of the average of the three historical proxy data sets from 1610 to 1890 and the combination of observed temperature data sets from 1889 to 2015. The correctness and accuracy is difficult to estimate, because the measurement based data sets deviate from each other up to 0.3°C in yearly values. The three selected temperature proxy graphs show the same kind of trends before 1890 explaining for example the temperature

decrease by the Tambora eruption in 1815. The temperature measurements starting from 1880 show almost as great differences as the proxy temperature graphs. The author has used the average of two different temperature measurement data sets published in 1975 [10] and the other in 1981 [12] for the period from 1889 to 1979. Because these data sets were published before the warming period since 1975, there has been no pressure to show any extra warming trend as it may now be a case. The author has used the UAH data set from 1980 onward. There was practically no difference between the temperature trends of UAH and GISS from 1979 to 2005 published before 2008 but thereafter the difference has increased to 0.26°C arousing doubts about the accuracy of latest version of GISS-16.

Many research studies show that Pacific Decadal Oscillation (PDO) phenomenon causes climate variations in the Pacific Basin and in the North America. The ENSO (El Niño-Southern Oscillation) causes also very clear climate impacts. The Atlantic Multi-decadal Oscillation (AMO) correlates with the sea surface temperature of the North Atlantic Ocean. By analyzing the long-term PDO index and the AMO index, it can be found that they follow quite well the general temperature trend of the Earth. For example, the high temperature periods of 1930's and 2000's happen at the same time as the maximum values of PDO and AMO index. The author's conclusion is that the oscillation phenomena like PDO and AMO are not the real root causes of the long-term climate change but they have the common origin.

The warming impact of GH gases has increased from 0% in 1750 to 37% in 2015. The Astronomic Harmonic Resonances (AHR) can explain the temperature peaks of the 1930's and the present warming period since 2000. The change in Sun activity explains the low temperatures during the LIA. Therefore, these climate forces should be included into the overall climate model.

Table 3. The summary of warming effects during the centuries, %

Century	Sun	GHGs	AHR	Volcanoes
1700-1800	99.5	4.6	-4.0	0.0
1800-1900	70.6	21.5	17.4	-9.4
1900-2000	72.5	30.4	-2.9	0.0
2015	46.2	37.3	16.6	0.0

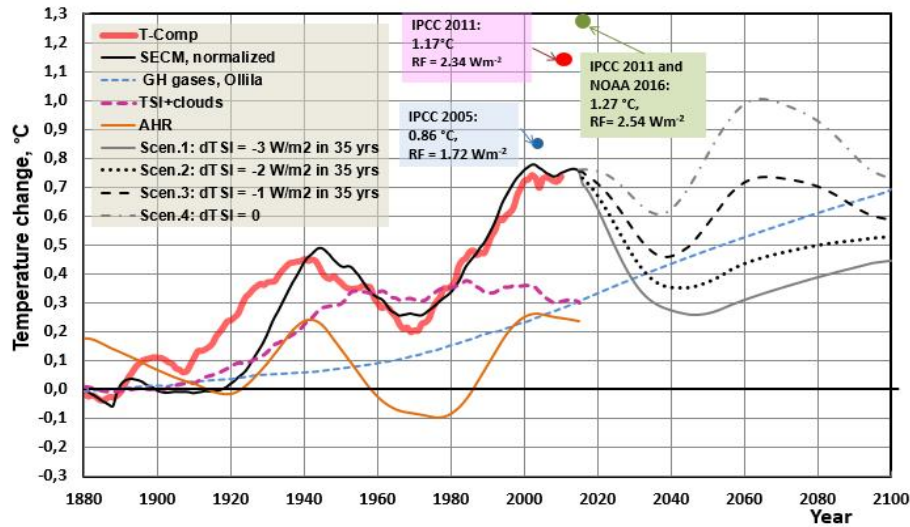


Fig. 9. Four scenarios from 2015 to 2100 using four different TSI change trends

5. CONCLUSIONS

The semi empirical climate model SECM has the coefficient of correlation $r^2 = 0.90$ and the standard error is 0.09°C . The SECM follows the ups and downs of the T-comp very well. The TSI variation is the major driving force of the temperature increase having the contribution of 71-73% during 19th and 20th centuries. Lean et al. [47] have carried out the correlation analysis between the NH surface temperature and the reconstructed solar irradiation and they found that a solar induced warming was 0.51°C from the LIA in the 1990's and the correlation was 0.86. This result is in line with the results of this study but the overall accuracy of SECM in this study is better, because of GHG and AHR effects included.

The Anthropogenic Global Warming (AGW) theory cannot explain any periods with decreasing temperatures. It is also obvious that the climate model of IPCC [1], which is based on the sums of the radiative forcings (RF), gives about 50% too high of a value in 2015. In this study, the author has used the formula of Ollila [22] in calculating the warming impact of CO_2 . This formula does not assume the constant relative humidity but the constant absolute humidity both in the radiative forcing and in the climate sensitivity parameter calculations.

The four scenarios calculated to 2100 show that the temperature would start to decrease after 2020 even though the TSI level would stay at the present level.

COMPETING INTERESTS

Author has declared that no competing interests exist.

REFERENCES

1. IPCC. The physical science basis, working group I contribution to the IPCC fifth assessment report of the intergovernmental panel on climate change. Cambridge University Press, Cambridge; 2013.
2. Briffa KR, Osborn TJ, Schweingruber FH, et al. Low-frequency temperature variations from a northern tree ring density network. *J Geophys Res.* 2001;106:2929–2941.
3. Moberg A, Sonechkin DM, Holmgren K, et al. Highly variable Northern Hemisphere temperatures reconstructed from low- and high-resolution proxy data. *Nature.* 2005; 433:613–617.
4. Lungqvist FC. A new reconstruction of temperature variability in the extra-tropical Northern Hemisphere during the last two millennia. *Geogr Ann.* 92 A. 2010;3:339–351.
5. UAH. UAH MSU temperature dataset. Available:[http://vortex.nsstc.uah.edu/data/msu/v6.0beta/tit/uahncdc It 6.0beta5.txt](http://vortex.nsstc.uah.edu/data/msu/v6.0beta/tit/uahncdc%206.0beta5.txt) (Accessed 10 Dec 2016)
6. HadCRUT4. Temperature dataset. Available:https://eosweb.larc.nasa.gov/project/erbe/erbe_table_41 (Accessed 10 Dec 2016)

7. GISS. Temperature dataset. Available:http://data.giss.nasa.gov/gistemp/tabledata_v3/GLB.Ts+dSST.txt42 (Accessed 10 Dec 2016)
8. Peterson TC. Monitoring and understanding changes in heat waves, cold waves, floods, and droughts in the United States. *Am Met Sc.* 2013;821-834.
9. Kelly MJ. Trends in extreme weather events since 1900 – An enduring conundrum for wise policy advice. *J Geogr Nat Disast.* 2016;155:1-7. DOI: 10.4172/2167-0587.1000155
10. National academy of sciences. Understanding climate change, a program for action. United States Committee for the Global Atmospheric Research Program, Washington D.C. 1975;239.
11. Budyko MI. The effect of solar variations on the climate of the Earth. *Tellus.* 1969; XXI:611-619.
12. Hansen J, Johnson D, Lacis A, et al. Climate impact of increasing atmospheric carbon dioxide. *Science* 1981;213:957-966.
13. Angell JK and Korshover J. Global temperature variation, surface – 100 mb: An update into 1977. *Mon Weather Rev.* 1978;106(6):755-770.
14. Soon W, Connolly R and Connolly M. Re-evaluating the role of solar variability on Northern Hemisphere temperature trends since the 19th century. *Earth-Sci Rev.* 2015;150:409-452.
15. IPCC. Climate response to radiative forcing, IPCC fourth assessment report (AR4), The physical science basis, contribution of working group I to the fourth assessment report of the intergovernmental panel on climate change. Cambridge University Press, Cambridge; 2007.
16. Myhre G, Highwood EJ, Shine KP, et al. New estimates of radiative forcing due to well mixed greenhouse gases. *Geophys Res Lett.* 1998;25:2715-2718.
17. Aldrin M, Holden M, Guttorp P, et al. Bayesian estimation on climate sensitivity based on a simple climate model fitted to observations of hemispheric temperature and global ocean heat content. *Environmetrics.* 2013;23:253-271.
18. Bengtson L, Schwartz SE. Determination of a lower bound on earth's climate sensitivity. *Tellus.* 2013;B:65. DOI:<http://dx.doi.org/10.3402/tellusb.v65i0.21533>
19. Otto A, Otto FEL, Allen MR, et al. Energy budget constraints on climate response. *Nature Geoscience.* 2016;6:415-416. Available:<http://dx.doi.org/10.1038/ngeo1836>.
20. Lewis NJ. An objective Bayesian improved approach for applying optimal fingerprint techniques to estimate climate sensitivity. *J Clim.* 2013; 26:7414-7429.
21. Harde H. Advanced two-layer climate model for the assessment of global warming by CO₂. *Open J Atm Clim Change.* 2014;1:1-50.
22. Ollila A. The potency of carbon dioxide (CO₂) as a greenhouse gas. *Dev Earth Sci.* 2014;2:20-30.
23. Ollila A. Warming effect reanalysis of greenhouse gases and clouds. *Ph Sc Int J.* 2017;13:1-13.
24. Ollila A. Cosmic theories and greenhouse gases as explanations of global warming. *J Earth Sci Geo Eng.* 2015;5:27-4.
25. Lean J. Solar Irradiance Reconstruction. IGBP PAGES/World data center for paleoclimatology data contribution series # 2004-035, NOAA/NGDC Paleoclimatology Program, Boulder CO, USA; 2004. Available:ftp://ftp.ncdc.noaa.gov/pub/data/paleo/climate_forcing/solar_variability/lean_2000_irradiance.txt
26. Hoyt DV, Schatten KH. A discussion of plausible solar irradiance variations, 1700-1992. *J Geo Res.* 1993;98:18895-18906.
27. Bard E, Raisbeck G, Yiou F, et al. Solar irradiance during the last 1200 years based on cosmogenic nuclides. *Tellus B.* 2000;52:985-992.
28. PMOD/WRC, Physikalisch-Meteorologisches Observatorium Davos. PMOD composite of the solar constant. Available:<https://www.pmodwrc.ch/pmod.php?topic=tsi/composite/SolarConstant>
29. Ollila A. Dynamics between clear, cloudy and all-sky conditions: cloud forcing effects. *J Chem Bio Phys Sci.* 2013;4:557-575.
30. McIntyre S and McKittrick R. Corrections to the Mann, et al. (1998) proxy data base and Northern Hemispheric average temperature series. *Ener & Environ.* 2003; 14:751–771.
31. Alley RB. The Younger Dryas cold interval as viewed from central Greenland. *Quaternary Sc Rev.* 2000;19:213-226.
32. Esper J, Duthorn E, Krusic PL, et al. Northern European summer temperature variations over the Common Era from

- integrated tree-ring density records. *J Quaternary Sc.* 2014;29(5):487-494.
33. Svensmark H. Influence of cosmic rays on earth's climate. *Ph Rev Let.* 1998;81: 5027-5030.
 34. Svensmark H, Bondo T and Svensmark J. Cosmic ray decreases affect atmospheric aerosols and clouds. *Geoph Res Lett.* 2009;36:L15101.
DOI: 10.1029/2009GL038429
 35. ISCCP. Radiation fluxes.
Available:<http://isccp.giss.nasa.gov/products/products.html39>
(Accessed 10 Dec 2016)
 36. Kauppinen J, Heinonen JT, Malmi PJ. Major Portions in Climate Change: Physical approach. *Int Rev Phy.* 2011;5: 260-270.
 37. Scafetta N. Empirical evidence for a celestial origin of the climate oscillations and its implications. *J Atmos Sol-Terr Phy.* 2010;72:951-970.
 38. Ermakov V, Okhlopkov V, Stozhkov Y, et al. Influence of cosmic rays and cosmic dust on the atmosphere and Earth's climate. *Bull Russ Acad Sc Ph.* 2009;73: 434-436.
 39. Gold T. Resonant orbits of grains and the formation of satellites. *Icarus.* 1975;25: 489-491.
 40. Wyatt MC, Dermott SF, Grogan K, et al. A unique view through the Earth's resonant ring, *Astrophysics with infrared surveys: A prelude to SIRTf.* ASP Conference Series. 1999;177:1-6.
 41. Dermott SF, Jayaraman S, Xu Y-L, et al. A circumsolar ring of asteroidal dust in resonant lock with the Earth. *Nature.* 1994; 369:719-723.
 42. NASA. Jet Propulsion Laboratory: Horizons Web-Interface.
Available:<http://ssd.jpl.nasa.gov/horizons.cgi>
(Accessed 1 Dec 2016).
 43. Wang J, Rossow WB and Zhang Y. Cloud vertical structure and its variations from a 20-yr global rawinsonde dataset. *J Climate.* 2016;13:3041-3056.
 44. Bradley RS. The explosive volcanic eruption signal in northern hemisphere continental temperature records. *Climate Change.*1998;12:221-243.
 45. Thomas MA. Simulation of the climate impact of Mt. Pinatubo eruption using ECHAM5. PhD Thesis, Hamburg University, Germany; 2008.
 46. Shepherd SJ, Zharkov SI, Zharkova VV. Prediction of solar activity from solar background magnetic field variations in cycles 21-23. *Astrophys J.* 2014;795: 46.
DOI: 10.1088/0004-637X/795/1/46
 47. Lean J, Beer J, Bradley R. Reconstruction of solar irradiance since 1610: Implication for climate. *Geoph Res Lett.* 1995;22(23): 3195-3198.

© 2017 Ollila; This is an Open Access article distributed under the terms of the Creative Commons Attribution License (<http://creativecommons.org/licenses/by/4.0>), which permits unrestricted use, distribution, and reproduction in any medium, provided the original work is properly cited.

Peer-review history:

*The peer review history for this paper can be accessed here:
<http://sciencedomain.org/review-history/19828>*